Model Compounds for the Oxidized Uteroferrin–Phosphate Complex. Syntheses, Crystal Structures, and Magnetic Properties of μ-Phosphato-, μ-Arsenato-, and μ-Chromato-Bridged Binuclear Iron(III) Complexes

Stefan Drüeke,[1a] Karl Wieghardt,*[1a] Bernhard Nuber,[1b] Johannes Weiss,[1b] Hans-Peter Fleischhauer,[1c] Stefan Gehring,[1c] and Wolfgang Haase[1c]

Contribution from the Lehrstuhl für Anorganische Chemie I, Ruhr-Universität, D-4630 Bochum, FRG, the Anorganisch-Chemisches Institut der Universität, D-6900 Heidelberg, FRG, and the Institut für Physikalische Chemie der Technischen Hochschule, D-6100 Darmstadt, FRG.
Received April 18, 1989

Abstract: A series of binuclear diiron(III) complexes of the type $L_2Fe_2(\mu\text{-}O)(\mu\text{-}XO_4)_2$ and $L_2Fe_2(\mu\text{-}XO_4)_3$ where L represents 1,4,7-trimethyl-1,4,7-triazacyclononane ($C_9H_{21}N_3$) and X = Cr^{VI}, P, and As were synthesized, and their electronic spectra and magnetic properties have been investigated. Complexes containing the (μ-oxo)bis(μ-oxoanion)diiron(III) core are possible structural model compounds for the oxidized form of the uteroferrin–phosphato complex: $[L_2Fe_2(\mu\text{-}O)(\mu\text{-}O_3P(OC_6H_5))_2]\text{-}NaClO_4\cdot 2H_2O$ (**2**) has been prepared from $[L_2Fe_2(\mu\text{-}O)(\mu\text{-}O_2CCH_3)_2](ClO_4)_2\cdot H_2O$ (**1**) via substitution of the μ-acetato bridges by $O_3P(OC_6H_5)^{2-}$, whereas $[L_2Fe_2(\mu\text{-}O)(\mu\text{-}HPO_4)_2]\cdot 3H_2O$ (**3**) and its arsenato analogue (**4**) were synthesized via hydrolysis of $LFeCl_3$ with Na_2HPO_4 or Na_2HAsO_4 in aqueous solution; $[L_2Fe_2(\mu\text{-}O)(\mu\text{-}CrO_4)_2]\cdot 4H_2O$ (**5**) was prepared analogously by using Na_2CrO_4. The triply bridged complexes, $L_2Fe_2(\mu\text{-}XO_4)_3$, formed in methanol via spontaneous self-assembly from $LFeCl_3$ and the corresponding oxoanion: XO_4 = $PO_3(OC_6H_5)^{2-}$ (**6**), HPO_4^{2-} (**7**), $HAsO_4^{2-}$ (**8**). The crystal structures of **2**, **5**, and $[L_2Fe_2(\mu\text{-}HAsO_4)_3]\cdot 6H_2O$ (**8**) have been determined by X-ray crystallography: (**2**) monoclinic $P2_1/c$, a = 15.583 (6) Å, b = 17.323 (8) Å, c = 17.167 (6) Å, β = 102.71 (3)°, Z = 4; (**5**) orthorhombic $Pnmm$, a = 8.209 (3) Å, b = 13.168 (6) Å, c = 14.546 (5) Å, Z = 2; (8) orthorhombic $Pcan$, a = 13.538 (7) Å, b = 16.143 (6) Å, c = 16.241 (7) Å, Z = 4. The diiron(III) centers in **2**, **3**, **4**, and **5** are strongly intramolecularly antiferromagnetically coupled: (**2**) J = −98 (1), (**3**) −80 (2), (**4**) −70 (4), (**5**) −124 (1) cm^{-1}. In contrast, in the triply bridged complexes, $L_2Fe_2(\mu\text{-}XO_4)_3$, only very weak antiferromagnetic coupling has been observed: (**6**) −3.5 (5), (**7**) −2.9 (6), (**8**) −1.0 (5) cm^{-1} ($H = -2JS_1\cdot S_2$; $S_1 = S_2 = {}^5/_2$; g = 2.00). The kinetics of the reaction of **1** with $Na_2[O_3P(OC_6H_5)]$ in alkaline aqueous solution (pH = 8) has been investigated. Formation of **2** was found to be zeroth-order in $O_3P(OC_6H_5)^{2-}$. The kinetics of the equilibration reaction of **1** in alkaline solution has also been studied at 25 °C: $k_{eq} = k_{obs} = k_{-2}[ac] + k_2K_1[OH^-]/(1 + k_2[OH^-])$, with K_1 = 3.2 × 10^5 M^{-1}, k_2 = 6.8 (2) × 10^{-3} s^{-1}, and k_{-2} = 0.5 (2) $M^{-1}s^{-1}$. This agrees with the following mechanism:

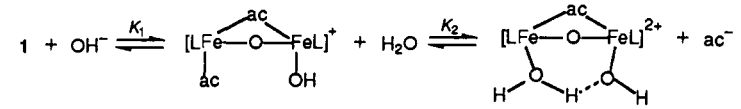

From equilibrium studies, K_1 and $K_2 = k_2/k_{-2}$ have been determined spectrophotometrically at 25 °C to be 5.5 (7) × 10^5 M^{-1} and 1.4 (5) × 10^{-2} M, respectively, in reasonable agreement with the values determined kinetically.

The mammalian purple acid phosphatases isolated from pig allantoic fluid or beef spleen catalyze the hydrolysis of phosphate esters under acidic conditions.[2,3] The enzymes have been shown to contain a binuclear non-heme-type iron unit. They exist in two forms, a violet, catalytically inactive, oxidized form containing two strongly antiferromagnetically coupled ($J \approx -100$ cm^{-1}) ferric ions[5-8] and a pink, active, reduced form which has been shown to contain a binuclear mixed-valence $Fe^{III}Fe^{II}$ active site.[8,9] The interaction of the active form with a variety of tetrahedral oxoanions such as phosphate,[10,11] arsenate, sulfate, molybdate, and tungstate[12,13] has been studied. It was found that these anions are tightly bound inhibitors. The anions bind to the reduced form of the enzyme, which in the presence of air forms the oxidized uteroferrin–oxoanion complex.[14-16] The most detailed studies are those in which the effect of phosphate on the active sites has been investigated, and some apparently conflicting results concerning the necessity of oxygen as an oxidant have been satisfactorily accommodated in the following scheme by Que and Scarrow.[2]

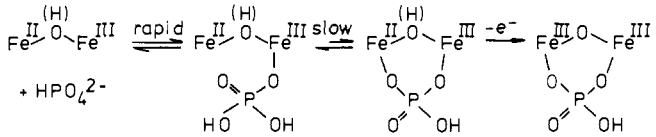

Thus, the available data suggest that a bidentate μ-HPO_4 and a

(1) (a) Ruhr-Universität, Bochum. (b) Universität Heidelberg. (c) Technische Hochschule, Darmstadt.
(2) (a) Antanaitis, B. C.; Aisen, P. *Adv. Inorg. Biochem.* **1983**, *5*, 111. (b) Que, L., Jr.; Scarrow, R. C. In *Metal Clusters in Proteins*; Que, L., Jr., Ed.; ACS Symposium Series 372; American Chemical Society: Washington, DC, 1988; p 152.
(3) Lippard, S. J. *Angew. Chem.* **1988**, *100*, 353; *Angew. Chem., Int. Ed. Engl.* **1988**, *27*, 344.
(4) Antanaitis, B. C.; Aisen, P.; Lilienthal, H. R. *J. Biol. Chem.* **1983**, *258*, 3166.
(5) Davis, J. C.; Averill, B. S. *Proc. Natl. Acad. Sci. U.S.A.* **1982**, *79*, 4623.
(6) Sinn, E.; O'Connor, C. J.; de Jersey, J.; Zerner, B. *Inorg. Chim. Acta* **1983**, *78*, L13.
(7) Mockler, G. M.; de Jersey, J.; Zerner, B.; O'Connor, C. J.; Sinn, E. *J. Am. Chem. Soc.* **1983**, *105*, 1891.
(8) Debrunner, P. G.; Hendrich, M. P.; de Jersey, J.; Keough, D. T.; Sage, J. T.; Zerner, B. *Biochim. Biophys. Acta* **1983**, *745*, 103.
(9) Lauffer, R. B.; Antanaitis, B. C.; Aisen, P.; Que, L., Jr. *J. Biol. Chem.* **1983**, *258*, 14212.
(10) Keough, D. T.; Beck, J. L.; de Jersey, J.; Zerner, B. *Biochem. Biophys. Res. Commun.* **1982**, *108*, 1643.
(11) Davis, J. C.; Lin, S. S.; Averill, B. A. *Biochemistry* **1981**, *20*, 4062.
(12) Antanaitis, B. C.; Aisen, P. *J. Biol. Chem.* **1985**, *260*, 751.
(13) Doi, K.; Gupta, R.; Aisen, P. *Recl. Trav. Chim. Pays-Bas* **1987**, *106*, 251; *J. Biol. Chem.* **1987**, *262*, 6982.
(14) Keough, D. T.; Dionysius, D. D.; de Jersey, J.; Zerner, B. *Biochem. Biophys. Res. Commun.* **1980**, *94*, 600.
(15) Antanaitis, B. C.; Aisen, P. *J. Biol. Chem.* **1984**, *259*, 2066.
(16) Burman, S.; Davis, J. C.; Weber, M. J.; Averill, B. A. *Biochem. Biophys. Res. Commun.* **1986**, *136*, 490.

0002-7863/89/1511-8622$01.50/0

μ-oxo group bridge two high-spin ferric ions in the fully oxidized uteroferrin–phosphato complex. From EXAFS spectra of the oxidized iron–phosphato complex of bovine and porcine uteroferrin,[17,18] Fe···Fe distances of ≈3.0 and 3.2 ± 0.1 Å, respectively, have been deduced; the corresponding Fe···P distances are 3.1–3.2 Å. The short Fe···Fe distance and the observed strong antiferromagnetic coupling ($-J > 150$ cm^{-1}) are taken as evidence for the presence of an Fe–O–Fe unit, although the ν_S(Fe–O–Fe) stretching frequency has not been detected by resonance Raman spectroscopy.[19]

In recent years, a number of low molecular weight complexes containing the (μ-oxo)bis(μ-carboxylato)diiron(III) core and a variety of tridentate amine capping ligands have been synthesized.[3] It has been shown that the carboxylato bridges in these model compounds are labile,[20-23] and in two instances, it has been demonstrated that oxoanions such as diphenyl phosphate[22] and carbonate[23] can replace these carboxylato bridges while retaining the Fe–O–Fe unit. Thus, $(HB(pz)_3)_2Fe_2O(O_2P(OC_6H_5)_2)_2$ and $L_2Fe_2O(CO_3)_2$ have been synthesized using the respective (μ-oxo)bis(μ-acetato)diiron(III) complexes as precursors. The μ-oxo groups in these compounds are also labile in protic media as is deduced from $H_2{}^{18}O$ isotope labeling studies.[22,24] Since oxoanions such as SO_4^{2-}, HPO_4^{2-}, $HAsO_4^{2-}$, VO_4^{3-}, MoO_4^{2-}, and WO_4^{2-} interact strongly with the reduced, pink form of uteroferrin and many physical properties of the oxidized form containing these bound oxoanions have been reported, it is of interest to prepare low molecular weight diiron(III) complexes that are structurally characterized and the physical properties of which are well understood. Comparison of the structural data and physical properties of model compounds with those reported for the biomolecules provides valuable information on the structural features of the diiron cores.

We wish to report here the syntheses, crystal structures, magnetic properties, and electronic spectra of two series of model complexes:

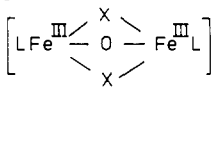

X = $O_3P(OC_6H_5)^{2-}$ (2)
HPO_4^{2-} (3)
$HAsO_4^{2-}$ (4)
CrO_4^{2-} (5)

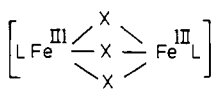

X = $O_3P(OC_6H_5)^{2-}$ (6)
HPO_4^{2-} (7)
$HAsO_4^{2-}$ (8)

In addition, we have investigated the solution behavior of $[L_2Fe_2(\mu\text{-}O)(\mu\text{-}O_2CCH_3)_2]^{2+}$ (**1**), and we have measured the kinetics of the reaction between **1** and $O_3P(OC_6H_5)^{2-}$ in alkaline aqueous solution, forming **2** quantitatively. A mechanism for the substitution of the μ-acetato bridges in **1** is proposed. This investigation represents the first kinetic study on the important (μ-oxo)bis(μ-carboxylato)diiron(III) core.

Experimental Section

Methods and Materials. The ligand 1,4,7-trimethyl-1,4,7-triazacyclononane (L) and the complexes $LFeCl_3$ and $[L_2Fe_2(\mu\text{-}O)(\mu\text{-}O_2CCH_3)_2](ClO_4)_2\cdot H_2O$ (**1**) have been prepared as described previously.[25,26] All other reagents were purchased from commercial sources and used without further purification.

$[L_2Fe_2O(PO_3(OC_6H_5))_2]\cdot NaClO_4\cdot 2H_2O$ (2). To an aqueous solution (20 mL) of **1** (0.50 g, 0.6 mmol) was added $Na_2[PO_3(OC_6H_5)]$ (0.25 g, 1.1 mmol). The solution was stirred at 60 °C for 30 min, after which time the solvent was removed under reduced pressure. The residue was extracted with acetonitrile (25 mL). A colorless precipitate was filtered off and discarded. To the green solution solid $NaClO_4\cdot H_2O$ (0.20 g) was added. After 3 days at ambient temperature, deep green crystals of **2** precipitated (0.40 g, 70%). Anal. Calcd for $C_{30}H_{56}N_6ClFe_2NaO_{15}P_2$: C, 37.00; H, 5.76; N, 8.64; Fe, 11.48; ClO_4, 10.22. Found: C, 37.0; H, 5.9; N, 8.6; Fe, 11.2; ClO_4, 10.5. UV–vis (CH_3CN): 627 nm (ϵ 190 cm^{-1} M^{-1}), 523 (270), 495 (sh), 482 (550), 416 (1450), 355 (sh), 332 (7030). IR (KBr, cm^{-1}): ν(PO) + ν(ClO) 1200 (sh), 1143 (vs), 1073 (s), 1000 (vs), 895 (s); ν_{as}(Fe–O–Fe) 694 (m).

$[L_2Fe_2O(HPO_4)_2]\cdot 3H_2O$ (3). To a solution of $LFeCl_3$ (0.50 g, 1.5 mmol) in water (20 mL) was added $Na_2HPO_4\cdot 2H_2O$ (2.0 g) at room temperature with stirring. The pH of this solution was adjusted to 10 by dropwise addition of 0.1 M NaOH whereupon the yellow-green color changed to deep green. The solvent water was removed under reduced pressure, and the solid residue was extracted with acetonitrile (25 mL). A colorless solid material was filtered off and discarded. From the solution, green microcrystals of **3** precipitated within 2 days at room temperature in a desiccator over H_2SO_4 (0.15 g, 39%). Anal. Calcd for $C_{18}H_{50}N_6Fe_2O_{12}P_2$: C, 30.16; H, 7.00; N, 11.73; Fe, 15.60. Found: C, 30.2; H, 7.2; N, 11.7; Fe, 16.0. UV–vis (CH_3CN): 962 nm (ϵ 5 cm^{-1} M^{-1}), 623 (196), 565 (sh), 523 (260), 494 (450), 483 (490), 419 (1510), 360 (6500), 330 (7400), 291 (6900), 240 (15.5 × 10^3). IR (KBr, cm^{-1}): ν(PO) 1130 (s), 1046 (vs), 1016 (vs); ν_{as}(Fe–O–Fe) 706 (m).

$[L_2Fe_2O(HAsO_4)_2]\cdot 3H_2O$ (4). This complex was prepared as described for **3** by using $Na_2HAsO_4\cdot 7H_2O$ (2.0 g) instead of $Na_2HPO_4\cdot 2H_2O$. Green microcrystals of **4** (0.15 g, ≈30%) were obtained. Anal. Calcd for $C_{18}H_{50}N_6As_2Fe_2O_{12}$: C, 26.86; H, 6.22; N, 10.44; Fe, 13.89. Found: C, 26.9; H, 6.4; N, 10.4; Fe, 14.1. UV–vis (CH_3CN): 614 nm (ϵ 155 cm^{-1} M^{-1}), 524 (217), 499 (370), 486 (380), 420 (sh), 360 (4050), 333 (4300), 290 (sh), 239 (15.6 × 10^3). IR (KBr, cm^{-1}): ν(AsO) 900 (vs), 855(s), 781 (s); ν_{as}(Fe–O–Fe) 702 (w).

$[L_2Fe_2O(CrO_4)_2]\cdot 4H_2O$ (5). To a solution of **1** (0.50 g, 6 mmol) in water (30 mL) was added Na_2CrO_4 (0.20 g, 12 mmol) with stirring at room temperature. The solution was allowed to stand in an open beaker for 2 days after which time a mass of dark red–brown crystals had precipitated, and the precipitate was filtered off, washed with an ether/ethanol mixture (4:1), and air-dried. Inspection of these crystals under a microscope revealed that two different crystalline forms had precipitated, which were manually separated. One type consisted of **5**, whereas the other was $[L_2Fe_2(\mu\text{-}CrO_4)_3]\cdot H_2O$ as was judged from their respective UV–vis spectrum and elemental analyses. In addition, both forms were analyzed by single-crystal X-ray analyses. When a few crystals of **5** were added to the above reaction mixture, crystals of **5** only precipitated within 24 h (0.10 g, ≈39%). Anal. Calcd for $C_{18}H_{50}N_6Cr_2Fe_2O_{13}$: C, 27.89; H, 6.46; N, 10.85; Fe, 14.43. Found: C, 27.9; H, 6.7; N, 10.9; Fe, 14.2. UV–vis (CH_3CN): 660 (sh) nm, 470 (sh), 374 (ϵ 10.0 × 10^3 cm^{-1} M^{-1}), 354 (9.7 × 10^3), 282 (1.5 × 10^4). IR (KBr, cm^{-1}): ν(CrO) 950 (s), 910 (s), 840 (s), 780 (s); ν_{as}(Fe–O–Fe): 700 (m).

$[L_2Fe_2(PO_3(OC_6H_5))_3]\cdot 4H_2O$ (6). To a solution of $LFeCl_3$ (0.50 g, 1.5 mmol) in dry methanol (40 mL) was added $Na_2[PO_3(OC_6H_5)]$. The yellow-green solution was stirred for 40 min at 50 °C. Within 12 h at room temperature, yellow-green crystals of **6** precipitated, which were collected by filtration, washed with CH_3CN/Et_2O (2:1), and air-dried (0.20 g, 30%). Anal. Calcd for $C_{36}H_{65}N_6Fe_2O_{16}P_3$: C, 34.53; H, 5.47; N, 8.06; Fe, 10.71. Found: C, 34.5; H, 5.3; N, 8.1; Fe, 11.0: UV–vis (CH_3CN): 300 (sh) nm (ϵ 3000 cm^{-1} M^{-1}). IR (KBr, cm^{-1}): ν(PO) 1230 (m), 1146 (s), 1010 (s), 897 (s).

$[L_2Fe_2(HPO_4)_3]\cdot 6H_2O$ (7). $LFeCl_3$ (0.50 g, 1.5 mmol) was dissolved in dry methanol (40 mL), and $Na_2HPO_4\cdot 2H_2O$ (0.1 g) was added. This solution was stirred at 50 °C for 40 min, and a colorless residue was filtered off. From the resulting solution, yellow-green crystals of **7** precipitated within 12 h at room temperature, which were collected by filtration, washed with a CH_3CN/Et_2O (2:1) mixture, and air-dried (0.30 g, 60%). Anal. Calcd for $C_{18}H_{57}N_6Fe_2O_{18}P_3$: C, 25.43; H, 6.76; N, 9.88; Fe, 13.14. Found: C, 25.7; H, 6.7; N, 10.2; Fe, 13.2. UV–vis

(17) Kauzlarich, S. M.; Teo, B. K.; Zirino, T.; Burman, S.; Davis, J. S.; Averill, B. A. *Inorg. Chem.* **1986**, *25*, 2781.
(18) Scarrow, R. C.; Que, L., Jr., work cited in ref 2.
(19) Averill, B. A.; Davis, J. C.; Burman, S.; Zirino, T.; Sanders-Loehr, J.; Loehr, T. M.; Sage, J. T.; Debrunner, P. G. *J. Am. Chem. Soc.* **1987**, *109*, 3760.
(20) Wieghardt, K.; Pohl, K.; Ventur, D. *Angew. Chem.* **1985**, *97*, 415; *Angew. Chem., Int. Ed. Engl.* **1985**, *24*, 392.
(21) Spool, A.; Williams, I. D.; Lippard, S. J. *Inorg. Chem.* **1985**, *24*, 2156.
(22) Armstrong, W. H.; Lippard, S. J. *J. Am. Chem. Soc.* **1985**, *107*, 3730.
(23) Drüeke, S.; Wieghardt, K.; Nuber, B.; Weiss, J. *Inorg. Chem.* **1989**, *28*, 1414.
(24) Armstrong, W. H.; Spool, A.; Papaefthymiou, G. C.; Frankel, R. B.; Lippard, S. J. *J. Am. Chem. Soc.* **1984**, *106*, 3653.
(25) Chaudhuri, P.; Winter, M.; Wieghardt, K.; Gehring, S.; Haase, W.; Nuber, B.; Weiss, J. *Inorg. Chem.* **1988**, *27*, 1564.
(26) (a) Chaudhuri, P.; Wieghardt, K.; Nuber, B.; Weiss, J. *Angew. Chem., Int. Ed. Engl.* **1985**, *24*, 778. (b) Hartman, J. R.; Rardin, R. L.; Chaudhuri, P.; Pohl, K.; Wieghardt, K.; Nuber, B.; Weiss, J.; Papaefthymiou, G. C.; Frankel, R. B.; Lippard, S. J. *J. Am. Chem. Soc.* **1987**, *109*, 7387.

Table I. X-ray Experimental Details for Complexes 2, 5, and 8

	2	5	8
empirical formula	$C_{30}H_{56}N_6ClO_{15}Fe_2NaP_2$	$C_{18}H_{46}N_6O_{11}Fe_2Cr_2$	$C_{18}H_{67}N_6As_3Fe_2O_{18}$
formula wt	972.9	774.3	992.2
crystal dimen, mm	0.26 × 0.30 × 0.31	0.34 × 0.46 × 0.48	0.45 × 0.45 × 0.30
radiation	Mo Kα (λ = 0.71073 Å)	Mo Kα (λ = 0.71073 Å)	Mo Kα (λ = 0.71073 Å)
temp, °C	22	22	22
space group	$P2_1/c$ (no. 14)	*Pnmm* (no. 59)	*Pcan* (no. 60)
a, Å	15.583 (6)	8.209 (3)	13.538 (7)
b, Å	17.323 (8)	13.168 (6)	16.143 (6)
c, Å	17.167 (6)	14.546 (5)	16.241 (7)
β, deg	102.71 (3)		
V, Å^3	4520.6	1572.4	3549.4
Z	4	2	4
ρ(calc), g/cm^3	1.43	1.62	1.84
μ, cm^{-1}	8.4	16.3	36.4
scan type	ω	ϑ–2ϑ	ω
ϑ–2ϑ range, deg	$3 < 2\vartheta < 60$	$3 < 2\vartheta < 60$	$3 < 2\vartheta < 60$
no. of reflcns measd	13500	2700	5739
no. of reflcns included	5065 ($I \geq 2.5\sigma(I)$)	1721 ($I > 2.5\sigma(I)$)	4257 ($I > 2.5\sigma(I)$)
corrections	Lorentz polarization, absorption	Lorentz polarization, absorption	Lorentz polarization, absorption
transmission factors	0.87–1.0	0.85–1.00	0.65–1.0
parameters refined	541	113	222
unweighted agreement factors[a]	0.062	0.053	0.030
weighted agreement factor[b]	0.055	0.051	0.029
convergence, largest shift/esd	0.25	0.25	0.02
high peak in final diff map, e$^-$/Å^3	0.70	1.1	0.3
goodness of fit[c]	2.68	4.36	2.62

[a] $R = \sum||F_o| - |F_c||/\sum|F_o|$. [b] $R_w = [\sum w(|F_o| - |F_c|)^2/\sum w|F_o|^2]^{1/2}$, $w = 1/\sigma^2(I)$. [c] $[\sum w(|F_o| - |F_c|)^2/(N_{observns} - N_{params})]^{1/2}$.

(CH_3CN): 310 (sh) nm (ε 3600 cm^{-1} M^{-1}). IR (KBr, cm^{-1}): ν(PO) 1150 (s, br), 1013 (s), 900 (m).

$[L_2Fe_2(HAsO_4)_3]\cdot 6H_2O$ (8). $Na_2HAsO_4\cdot 7H_2O$ (0.90 g; 2.9 mmol) was dissolved in H_2O (25 mL), and $LFeCl_3$ (0.3 g, 0.9 mmol) was added. This solution was stirred at 70 °C for 1–2 h until the color had changed to yellow. After filtration, the solvent was removed under reduced pressure at 70 °C. The residue was dissolved in methanol (50 mL). After filtration, the clear solution was allowed to stand at room temperature for 12 h within which time yellow crystals of X-ray quality slowly precipitated (0.15 g, 50%). Anal. Calcd for $C_{18}H_{57}N_6As_3Fe_2O_{18}$: C, 22.01; H, 5.85; N, 8.56; Fe, 11.37. Found: C, 22.3; H, 5.7; N, 8.7; Fe, 11.7. UV–vis (CH_3CN): 330 (sh) nm (ε 2950 cm^{-1} M^{-1}). IR (KBr, cm^{-1}): ν(AsO) 932 (vs), 910 (ms), 881 (vs).

X-ray Crystallography. Intensities and lattice parameters of a green, column-shaped crystal of **2** and a yellow, pyramidal crystal of **8** were measured on an AED II (Siemens) diffractometer, whereas those of a brown cubic crystal of **5** were measured on a Syntex R3 diffractometer. Crystal parameters and details of the data collection and reduction are given in Table I. Lattice parameters for all complexes were obtained from a least-squares fit to the setting angles of 35 (for **2**) and 25 (for **5** and **8**) reflections with $6° \leq 2\vartheta \leq 27°$. Empirical absorption corrections (ψ scans) were carried out in each case (eight, six, and eight reflections, $10.3° < 2\vartheta < 40°$, $16.2° \leq 2\vartheta \leq 26.6°$, $5° < 2\vartheta < 60°$ for **2**, **5**, and **8**, respectively). All structures were solved by standard Patterson and difference Fourier methods and refined[27] with anisotropic thermal parameters for all non-hydrogen atoms. Neutral atom scattering factors and anomalous dispersion corrections for non-hydrogen atoms were taken from ref 28 and hydrogen atom scattering factors from ref 29. All methylene and phenyl hydrogen atoms were placed at calculated positions with d(C–H) = 0.96 Å, while the methyl groups were treated as rigid bodies, each with three rotational variables. The function minimized during refinement was $\sum w(|F_o| - |F_c|)^2$ where $w = 1/\sigma^2(I)$.

Some special features of the structure determinations are as follows. The positions of the hydrogen atoms of the water molecules of crystallization in crystals of **2** and **5** have not been located. In contrast, the final difference Fourier map of **8** revealed residual electron density (0.8–1.2 e/Å^3) in the vicinity of the water molecules (0.8–1.1 Å) which could not be refined as hydrogen atoms, but these peaks were included with fixed positional and fixed isotropic thermal parameters in the final refinement cycle as hydrogen atoms whereupon the convergence factors decreased by 0.02. These positions are given in Table S13 (supplementary material); they are all in chemically reasonable positions for hydrogen atoms that form an extended hydrogen bonding scheme shown in Figure 4. Final positional parameters are presented in Tables II, III, and IV of the supplementary material for **2**, **5**, and **8**, respectively.

Physical Measurements. Optical and Infrared Spectroscopy. Electronic absorption spectra in the 200–1200-nm range were recorded with a Perkin-Elmer Lambda 9 spectrophotometer, while infrared spectra were recorded with a Perkin-Elmer Model 1702 spectrometer.

Magnetic Susceptibility Measurements. Solid-state magnetic susceptibilities of powdered samples were measured in the 4–300 K range by using a Faraday-type magnetometer. Pascal's[30,31] constants were used to calculate the diamagnetic correction. The theoretical expression (vide infra) was fit to the data by the least-squares method by using a locally written program.

Kinetic Studies. The kinetics of the equilibrium reaction of **1** in alkaline aqueous solutions were measured by using conventional spectrophotometry monitoring the decrease of absorption at 460 nm as a function of time. A Unicam SP 1700 spectrophotometer interfaced to a Commodore VC 64 computer was used for data acquisition and analyses. Pseudo-first-order rate constants were calculated with a least-squares program[32] where the absorbance at the beginning ($t = 0$) and after the completed reaction ($t = \infty$) were treated as variables. The observed and calculated values differed only within the uncertainty of the last digit of the readings of the instrument. The kinetics of the reaction of **1** with $O_3P(OC_6H_5)^{2-}$ at pH 8 were measured analogously. The pH of solutions was adjusted to the desired values by using borate/NaOH buffers (I = 0.25 M). In a few experiments, some noncoordinating buffers based on substituted lutidines[33] were used to establish that the rates were independent of the nature of the buffer used here.

Results and Discussion

Synthesis. It is now well established that diiron complexes containing the (μ-oxo)bis(μ-carboxylato)diiron(III) core readily assemble in aqueous solution from mononuclear, e.g., $LFeCl_3$, or binuclear precursors, e.g., $[Cl_3FeOFeCl_3]^{2-}$, in the presence of carboxylic acids and tridentate capping amine ligands such as hydrotris(pyrazolyl)borate ($HB(pz)_3$), 1,4,7-triazacyclononane, 1,4,7-trimethyl-1,4,7-triazacyclononane, and other ligands.[3] It

(27) All computations were carried out on an ECLIPSE computer using the SHELXTL program package (G. M. Sheldrick, Göttingen).
(28) *International Tables for X-ray Crystallography*; Kynoch: Birmingham, England, 1974; Vol. IV, pp 99, 149.
(29) Stewart, R. F.; Davidson, E. R.; Simpson, W. T. *J. Chem. Phys.* **1965**, *42*, 3175.
(30) Carlin, R. L. In *Magnetochemistry*; Springer-Verlag: New York, 1986; p 3.
(31) O'Connor, C. J. *Progr. Inorg. Chem.* **1982**, *29*, 203.
(32) DeTar, D. *Comput. Chem.* **1979**, *2*, 99.
(33) Bips, U.; Elias, H.; Hanröder, M.; Kleinhans, G.; Pfeifer, S. *Inorg. Chem.* **1983**, *22*, 3862.

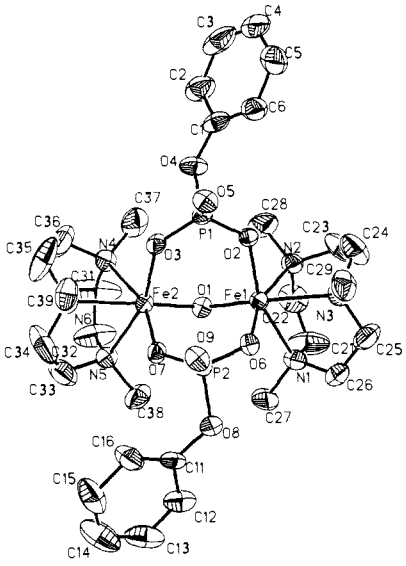

Figure 1. Structure of the neutral molecule in **2**, showing 40% probability thermal ellipsoids and the atom labeling scheme.

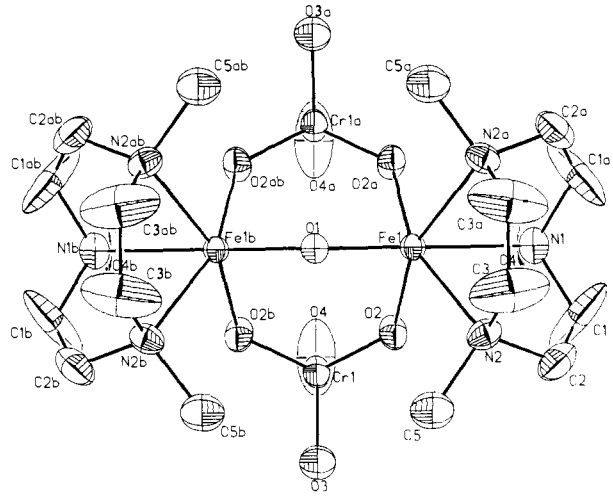

Figure 2. Structure of the neutral molecule in **5**, showing 40% probability thermal ellipsoids and the atom labeling scheme.

has also been demonstrated that the μ-carboxylato bridges are generally labile in aqueous solution and aprotic solvents and may be replaced by other bidentate bridging groups.[20-23] Lippard and Armstrong have used this strategy to prepare $Fe_2O\{O_2P(OC_6H_5)_2\}_2(HB(pz)_3)_2$, a phosphodiester-bridged complex, from $(HB(pz)_3)_2Fe_2O(O_2CCH_3)_2$ in CH_2Cl_2 by addition of $(C_6H_5O)_2PO_2H$.[22] Chaudhuri et al., on the other hand, have recently shown that binuclear complexes *without* a μ-oxo bridge but with three identical CrO_4^{2-}, MoO_4^{2-}, and WO_4^{2-} bridging groups formed from $LFeCl_3$ in aqueous solution in the presence of these oxoanions.[25] The complexes $[LFe(\mu\text{-}XO_4)_3FeL]$ have been synthesized (X = Cr, Mo, W) and the tris(μ-chromato) complex has been characterized by X-ray crystallography.

Following Lippard's procedure, we have found that $[L_2Fe_2O(\mu\text{-}O_2CCH_3)_2)](ClO_4)_2\cdot H_2O$ (**1**) dissolved in water reacts readily with the phosphomonoester $[O_3P(OC_6H_5)]^{2-}$, affording in good yields the neutral complex $L_2Fe_2O(O_3P(OC_6H_5)_2$ which was isolated as the green $NaClO_4$ mixed salt in crystalline form. Crystals of **2** were suitable for X-ray crystallography (vide infra). Hydrolysis of $LFeCl_3$ in alkaline aqueous solution (pH $\approx$ 10) in the presence of HPO_4^{2-} or $HAsO_4^{2-}$ gave in reasonable yields the green neutral species $[L_2Fe_2O(PO_4H)_2]\cdot 3H_2O$ (**3**) and $[L_2Fe_2O(AsO_4H)_2]\cdot 3H_2O$ (**4**), respectively, as crystalline materials. In the presence of Na_2CrO_4, the binuclear complex (**1**) reacts in water with substitution of the μ-acetato bridges, forming red-brown crystals of $[L_2Fe_2O(CrO_4)_2]\cdot 4H_2O$ (**5**) and, at the same time, with substitution of the μ-acetato *and* the μ-oxo bridges, generating red-brown crystals of $[L_2Fe_2(CrO_4)_3]\cdot H_2O$. Both forms were separated manually under a microscope; their UV–vis spectra differ significantly (see below), and therefore, the forms are readily distinguished. It was found that the formation of **5** as the only crystalline product could be achieved when a few crystals of **5** were added to the above reaction mixture. This implies that in solution **5** and the tris(μ-chromato) species are in equilibrium. Induced precipitation of **5** leads to nearly quantitative formation of **5**.

Spontaneous self-assembly of (μ-oxo)diiron(III) complexes from mononuclear precursors, e.g., $LFeCl_3$, requires the presence of water and a proton acceptor. Therefore, it should be possible to synthesize triply bridged diiron(III) complexes without a μ-oxo group in nonaqueous solvents with only small amounts of water present. Indeed, the reaction of $LFeCl_3$ in dry methanol with $Na_2[O_3P(OC_6H_5)]$, $Na_2HPO_4\cdot 2H_2O$, or $Na_2HAsO_4\cdot 7H_2O$ affords clear yellow solutions from which yellow crystals of $[L_2Fe_2(O_3P(OC_6H_5))_3]\cdot 4H_2O$ (**6**), $[L_2Fe_2(HPO_4)_3]\cdot 6H_2O$ (**7**), and $[L_2Fe_2(HAsO_4)_3]\cdot 6H_2O$ (**8**) crystallized.

Description of Structures. $[L_2Fe_2O(O_3P(OC_6H_5))_2]NaClO_4\cdot 2H_2O$ (2). The structure of the neutral binuclear iron(III) complex in crystals of **2** and the atom labels are shown in Figure 1; selected bond distances and angles are summarized in Table V of the supplementary material. Two bidentate dianions of monophenylphosphate(2–) bridge the (μ-oxo)diiron(III) core, and the resulting $\{Fe_2O\{O_3P(OC_6H_5)\}_2\}^0$ unit is capped by two 1,4,7-trimethyl-1,4,7-triazacyclononane ligands. The structure is very similar to Lippard's neutral complex $[Fe_2O\{O_3P(OC_6H_5)_2\}_2(HB(pz)_3)_2]$ where two monoanions of $O_2P(PC_6H_5)_2^-$ form bridges and the overall charge is neutralized in this instance by two hydrotris(pyrazolyl)borate(1–) ligands and an oxo group.[22] The average $Fe\text{–}O_{oxo}$ bond length of 1.818 Å in **2** is longer than the corresponding distance in the (μ-oxo)bis(μ-acetato)diiron(III) species (**1**) (1.800 Å).[26b] The Fe–N distances in trans positions with respect to the μ-oxo bridge are significantly longer than the corresponding bonds cis to the $Fe\text{–}O_{oxo}$ group ($\Delta[(Fe\text{–}N_{trans}) - (Fe\text{–}N_{cis})] = 0.05$ Å). The Δ value is 0.07 Å for **1**. Thus, the μ-oxo groups clearly exhibit a pronounced trans influence which increases with decreasing $Fe\text{–}O_{oxo}$ distances. The larger Fe–O–Fe angles, 123.2 (3)° vs 119.7 (1)°, and resulting greater Fe···Fe separations 3.198 (2) vs 3.120 Å, in **2** as compared to **1** are presumably due to the increased O···O separation in phosphate compared to carboxylate ligands. Similar observations have been reported for Lippard's diphenylphosphato- and diphenylacetato–diiron complexes.[22] There are three distinctly different P—O distances observed in the μ-phenylphosphato bridges: a short P=O bond at 1.478 Å (average) a medium distance at 1.512 Å (P—O—Fe), and a long one at 1.627 Å (P—O—C_6H_5). The average nonbonding Fe···P distance is 3.209 Å.

The terminal atoms O5 and O9 of both bridging phenylphosphato groups are bound to the sodium cation which, in addition, is coordinated to a water molecule of crystallization (O_w1). The ClO_4^- anion is in close proximity to Na^+ (Na···Cl 3.643 (5) Å), and one ClO_4^- oxygen atom (O11) is bound to the sodium cation (Na–O11 2.310 (3) Å). The coordination geometry of the sodium atom is therefore best described as distorted tetrahedral.

Interestingly, the analyses of the second-shell EXAFS spectra of bovine and porcine oxidized uteroferrin phosphate complexes have identified Fe···Fe distances at 3 and 3.2 ± 0.1 Å and Fe···P distances at 3.1–3.2 Å.[17,18] The corresponding distances in **2** and in Lippard's diphenylphosphato complex[22] are in excellent agreement with these values. These compounds obviously model the spatial arrangement of the diiron core in the enzymes well, and they indicate that the diiron core in the biomolecule is at least doubly bridged including a μ-oxo bridge for which direct resonance Raman spectroscopic evidence is lacking.[19]

$[L_2Fe_2O(CrO_4)_2]\cdot 4H_2O$ (5). Figure 2 shows the structure of the neutral binuclear complex **5**; selected bond distances and angles are given in Table VI of the supplementary material. The $L_2Fe_2O(CrO_4)_2$ complex has crystallographically required *mm* symmetry. Each iron atom has a distorted octahedral coordination sphere comprised of two bridging bidentate chromates, a bridging

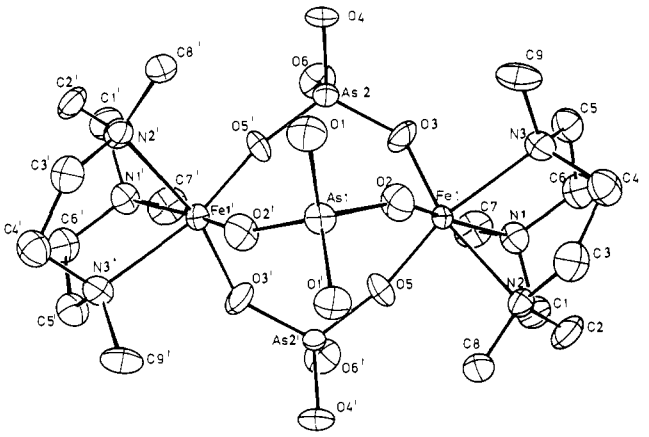

Figure 3. Structure of the neutral molecule in **8**, showing 40% probability thermal ellipsoids and the atom labeling scheme.

μ-oxo group, and a tridentate facially coordinating amine ligand. The site symmetry *mm* is not compatible with the ($\lambda\lambda\lambda$)- or ($\delta\delta\delta$)-ring conformation of the three five-membered chelate rings, FeNCCN, of the capping macrocycle. Consequently, the complex is disordered in crystals of **5** which is borne out by physically meaningless, large anisotropic temperature factors of the methylene carbon atoms and unrealistic short C–C bond lengths (1.36–1.37 Å). This feature is often encountered in crystal structures of transition-metal compounds containing coordinated 1,4,7-triazacyclononane ligands and N-substituted derivatives.[26b,34]

The Fe–O_{oxo} bond length is 1.819 (2) Å, which is longer as compared to other μ-oxo–diiron(III) complexes where bond distances in the range 1.78–1.80 Å have been observed. The Fe–O_{oxo} structural trans influence is quite small (Δ[(Fe–N_{trans}) – (Fe–N_{cis})] = 0.029 Å). The nonbonding Fe···Fe distance is 3.285 Å, which again is greater than the corresponding distance in the carboxylate bridged analogue (**1**) due to the larger O···O separation of the chromates as compared to carboxylates.

The chromium atoms in **5** are in a distorted tetrahedral environment of four oxygen atoms. There are three significantly different Cr–O distances at 1.560 (6), 1.615 (6), and 1.664 (3) Å. The shortest terminal distance exhibits considerable double bond character, whereas the two long distances of Cr1–O2 and Cr1–O2′ are single bonds (O2 and O2′ are also bound to iron atoms, respectively). The terminal oxygen atom, O3, is involved in a O3···H–O_w2 hydrogen contact (O3···O_w2 2.876 (7) Å), whereas O4 does not form a hydrogen bond. The symmetry of the μ-CrO_4 group is less than C_{2v}, which would be anticipated for a bidentate μ-chromato bridge. Other O–H···O contacts of the water molecules of crystallization are summarized in Table VI of the supplementary material.

It is of interest to compare the structure of **5** with the previously reported structure of $[L_2Fe_2(\mu\text{-}CrO_4)_3]\cdot H_2O$ which contains three bidentate chromato bridges and no μ-oxo bridge.[25] The Fe···Fe distance in the latter increases to 4.552 (5) Å; the Fe–N distances range from 2.201 (9) to 2.241 (10) Å. Within the experimental uncertainty, these bonds are equivalent; the mean value of 2.224 Å agrees well with the Fe–N_{cis} bond lengths in **5**. The average Fe–O_{Cr} distance of 1.897 Å in the tris(μ-chromato) complex is slightly shorter than the Fe–O_{Cr} distance in **5** of 1.957 (3) Å. In $[L_2Fe_2(\mu\text{-}CrO_4)_3]\cdot H_2O$, only two different Cr—O bond lengths at 1.678 and 1.574 Å are observed for those oxygens coordinated to iron atoms and the terminal Cr=O groups, respectively. The bidentate μ-CrO_4 groups possess C_{2v} symmetry.

$[L_2Fe_2(HAsO_4)_3]\cdot 6H_2O$ (8). The molecular structure and the atom labeling scheme of **8** are shown in Figure 3; selected bond distances and angles are given in Table VII of the supplementary material. Three arsenato ions bridge two iron(III) ions in a bidentate fashion. The neutral molecule in **8** has crystallographically required C_2 symmetry. The Fe coordination geometry

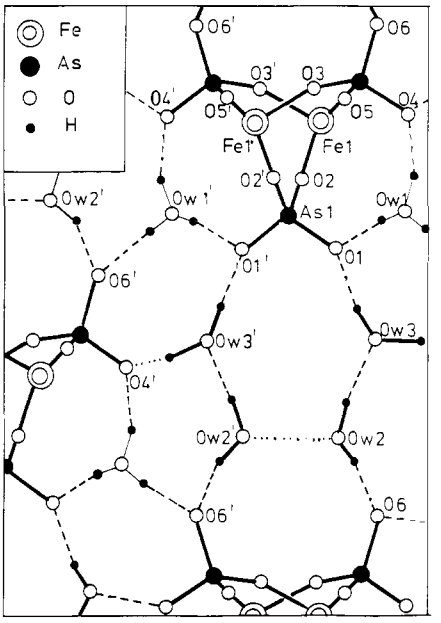

Figure 4. Probable hydrogen bonding scheme in **8**. The proton between O_w2 and O_w2′ has not been located. The amine ligands have been omitted for the sake of clarity.

Table VIII. O–H···O Contacts for $[L_2Fe_2(HAsO_4)_3]\cdot 6H_2O$ (**8**)

O_w1–O1	2.639 (3)	O_w2–O_w2′	2.660 (4)
O_w1–O4	2.780 (3)	O_w2–O_w3	2.772 (4)
O_w1–O6	2.805 (3)	O_w2–O6	2.656 (3)
O_w3–O_w2	2.772 (3)	O_w3–O1	2.824 (4)
O_w3–O4	2.824 (4)		

is distorted octahedral with three nitrogen atoms from each capping macrocycle and three oxygen atoms from three bridging arsenato groups. The three Fe–N distances ranging from 2.232 to 2.246 (4) Å are equivalent within experimental error; they agree well with those in the tris(μ-chromato) complex and the Fe–N_{cis} distances in **1**, **2**, and **8**. They are indicative of high-spin ferric ions. The Fe–O bond lengths range from 1.903 (4) to 1.944 (4) Å. The Fe···Fe separation in **8** is 4.456 (3) Å, which may be compared with a value of 4.552 (5) Å in $[L_2Fe_2(\mu\text{-}CrO_4)_3]\cdot H_2O$.

An interesting facet of the structure of **8** is the observation that the As—O distances of the apparently terminal As=O groups are *longer* than the corresponding bonds of the As—O—Fe units; the average difference between these two types of As—O bonds is 0.047 Å,[35] which is significantly larger than three times the estimated standard deviation of these bond lengths (3σ = 0.012 Å). In contrast, in **2**, **5**, and $[L_2Fe_2(\mu\text{-}CrO_4)_3]\cdot H_2O$, the comparable terminal X=O bonds were found to be *shorter* than the X—O bonds of the X—O—Fe units (X = P, Cr). Simple charge neutrality arguments have lead us to assign hydrogenarsenato(2–) bridges in **8**, which compensate the six positive charges of two ferric ions. In the solid state, this is obviously not the case, as is discussed now.

From the final difference Fourier map, 14 residual electron density peaks have been located, all of which are in the vicinity of oxygen atoms of the molecules of water and crystallization. Charge neutrality requires 15 oxygen-bound hydrogen atoms. The proton between O_w2 and O_w2′ has not been found. The distances of these peaks from the oxygen atoms range from 0.8 to 1.1 Å. It is therefore reasonable to assign these peaks to hydrogen atoms. Attempts to refine the positional parameters failed, but the tentative hydrogen-bonding scheme derived from these positions is chemically reasonable and is shown in Figure 4. The O···O distances of these O–H···O contacts range from 2.639 (3) to 2.824

(34) Chaudhuri, P.; Wieghardt, K. *Progr. Inorg. Chem.* **1987**, *35*, 329.

(35) In $[Na_2(OH_2)_7][AsO_3OH]$, the terminal As=O bond lengths are 1.66 Å, whereas the As—OH bond is 1.73 Å. Baur, W. H.; Khan, A. A. *Acta Crystallogr.* **1970**, *B26*, 1584. The As–O distances in **8** indicate that a formulation as bridging $HAsO_4^{2-}$ is not appropriate.

Table IX. Results of Magnetic Measurements and Comparison with Structural Data of Diiron(III) Complexes

complex	Fe–O_{oxo}, Å	Fe–O–Fe, deg	Fe···Fe, Å	J,[a] cm^{-1}	g	p, %	ref
		A. μ-Oxo-Bridged Species					
$[L_2Fe_2O(O_2CCH_3)_2](ClO_4)_2 \cdot H_2O$	1.800 (3)	119.7 (1)	3.12	−119	2.0	0.7	26b
$[L_2Fe_2O(CO_3)_2] \cdot 4.25H_2O$	1.820 (3)	113.8 (4)	3.048 (2)	−91 (1)	1.999	0.04	23
2	1.817 (5)	123.2 (3)	3.198 (3)	−98 (1)	2.06	0.14	this work
3				−80 (1)	2.01	1.26	this work
4				−70 (4)	2.01	2.6	this work
5	1.819 (2)	129.1 (3)	3.285 (4)	−124 (2)	2.06	0.01	this work
		B. Tris(μ-Oxoanion) Species					
6				−3.5 (2)	1.99	2.4	this work
7				−2.9 (6)	2.02	0.7	this work
8			4.456 (3)	−1.0 (2)	1.98	1.0	this work
$L_2Fe_2(MoO_4)_3$				−4.4 (2)	2.02	1.1	25
$L_2Fe_2(CrO_4)_3$			4.552 (5)	−7.5 (2)	2.00	0.4	25

[a] Spin-exchange coupling constant $H = -2J\hat{S}_1 \cdot \hat{S}_2 (S_1 = S_2 = {}^5/_2)$.

(4) Å (Table VIII), which is typical for hydrogen bonding between two oxygen atoms.

Interestingly, according to this scheme, one oxygen (O_w1) is bound to three protons, forming thus a H_3O^+ cation. This cation is hydrogen bonded to two "terminal" As–O oxygen atoms (O1 and O4) of two arsenato bridges of the same neutral molecule in **8** and a third terminal arsenato oxygen atom (O6) of a second molecule. The geometry of H_3O^+ is pyramidal (H–O–H angles 111.1°, 111.2°, and 122.4°). In addition, each of the terminal arsenato oxygen atoms forms a second hydrogen bond: O6 to O_w2, O4 to O_w3, and O1 to O_w3. Thus, each terminal arsenato oxygen atom forms *two* O–H···O_{As} contacts which cause the observed lengthening of the As–O_t bonds.

The remaining water molecules of crystallization form a $[H_9O_4]^+$ cation. The $[H_9O_4]^+$ cation may be envisaged as being composed of (a) a H_3O^+ cation bound to three additional water molecules via hydrogen bonding or, alternatively, (b) a $[H_5O_2]^+$ unit that is bound to two additional H_2O. The O_w2–O_w2' distance of 2.660 Å is relatively long for an $[H_5O_2]^+$ unit.[36] In $[H_5O_2]Cl \cdot H_2O$,[37] an O···O distance of 2.41 Å and in $[H_5O_2]ZnCl_3$[38] only 2.38 Å have been observed. The O···O distances in $[H_3O]^+ \cdot 3H_2O$ range from 2.50 to 2.68 Å.[36] It is not possible to clearly discern between (a) and (b) in **8**, but the observed $O_w2' \cdots O_w2$ distance would favor a formulation like $[H_3O]^+ \cdot 3H_2O$. Thus, **8** may be reformulated as $[H_3O]_2[H_9O_4][L_2Fe_2(\mu\text{-}AsO_4)_3]$.

Electronic Spectra and Magnetic Properties. The electronic spectra of complexes containing a (μ-oxo)bis(μ-carboxylato)diiron(III) core both in low molecular weight model compounds and in the biomolecule hemerythrin display some remarkable features.[3] In general, they exhibit a series of fairly intense d–d transitions in the visible and near-IR in the range 500–1200 nm and, more importantly and characteristically, two to three intense absorption maxima in the near-UV in the range 300–480 nm with absorption coefficients > 1000 M^{-1} cm^{-1}. These latter bands have been assigned to simultaneous pair excitation (SPE) bands[39] or, alternatively, Fe–O_{oxo} charge-transfer (CT) bands. Recently Sanders-Loehr et al.[40] have presented evidence that the latter assignment is probably more appropriate. Substitution of the acetato bridges by diphenylphosphato or carbonato bridges does not change this pattern significantly.[22,23]

Figure 5a shows the spectrum of $[L_2Fe_2(\mu\text{-}O)(\mu\text{-}HPO_4)_2] \cdot 3H_2O$ (**3**) as an illustrative example of the present series of $L_2Fe_2(\mu\text{-}O)(\mu\text{-}XO_4)_2$ complexes. It fits well to the pattern described above. Upon substitution of the μ-oxo group by a third XO_4 bridge, the electronic spectra change dramatically. Thus, in the spectra of **6**, **7**, and **8** only one broad CT band in the range 320–350 nm is observed as a shoulder. Figure 5b shows the spectrum of $[L_2Fe_2(HPO_4)_3] \cdot 6H_2O$ (**7**) which is to be compared with that of **3**. The d–d transitions in the visible are not observable in these triply XO_4-bridged species, which is probably due to the weak antiferromagnetic coupling of the high-spin ferric ions in these compounds as compared to strong coupling in μ-oxo-bridged complexes. The intensity of the spin-forbidden d–d transitions decreases considerably ($\epsilon < 1$) upon substitution of the μ-oxo bridge by other ligands, which do not facilitate the superexchange

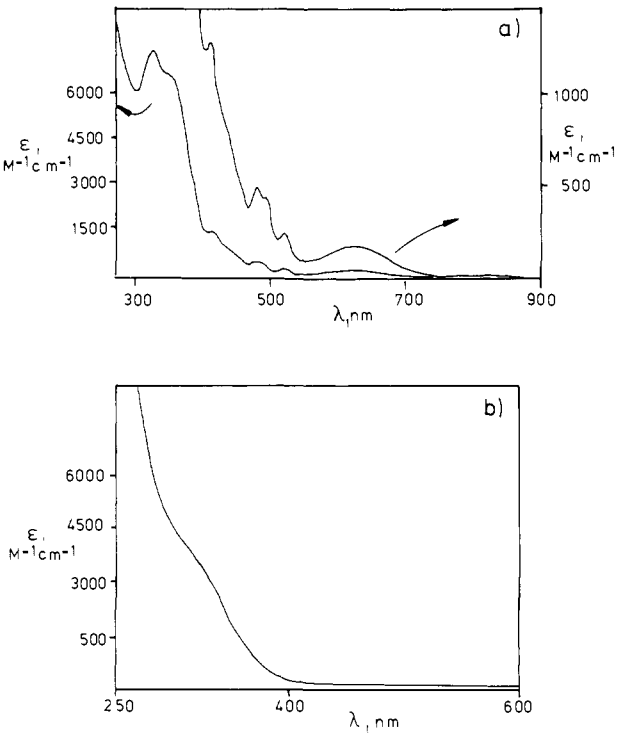

Figure 5. Electronic spectra of (a) **3** and (b) **7** in acetonitrile at 20 °C.

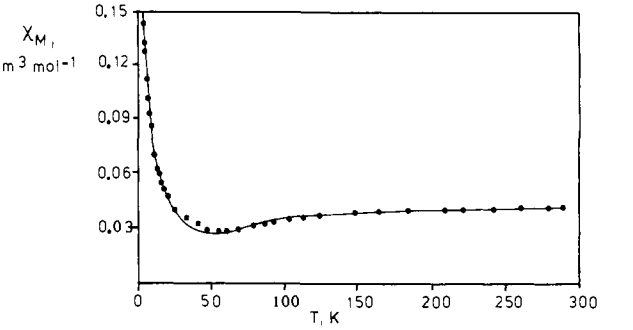

Figure 6. Plot of χ_M vs T for **3**. (●) Experimental data; (—) fit by the expression given in the text.

(36) Wells, A. F. *Structural Inorganic Chemistry*; Oxford University Press: New York, 1984; pp 838–875.
(37) Lundgreen, J.-O.; Olovsson, I. *Acta Crystallogr.* **1967**, *23*, 971.
(38) Follner, H. *Acta Crystallogr.* **1970**, *B26*, 1544.
(39) Schugar, H. J.; Rossman, G. R.; Barraclough, C. G.; Gray, H. B. *J. Am. Chem. Soc.* **1972**, *94*, 2683.
(40) Sanders-Loehr, J.; Wheeler, W. D.; Shiemke, A. K.; Averill, B. A.; Loehr, T. M. *J. Am. Chem. Soc.*, submitted for publication.

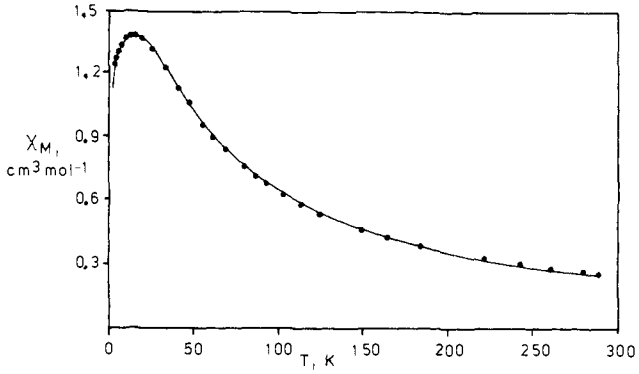

Figure 7. Plot of χ_M vs T for **8**. (●) Experimental data; (—) fit by the expression described in the text.

mechanism as efficiently as μ-oxo bridges. The effect of exchange coupling on optical spectra and intensity enhancement of bands has recently been discussed in depth by McCarthy and Güdel.[41]

Magnetic susceptibility measurements for powdered samples of complexes were made by using the Faraday method in the range 4.2–290 K. The data were excellently fit by the expression[26b,31] for χ_M vs T derived from the spin-exchange Hamiltonian, $H' = -2J\hat{S}_1\cdot\hat{S}_2$, with $S_1 = S_2 = {}^5/_2$ and $g \approx 2.0$. For a satisfactory fit, it was necessary to include a Curie–Weiss term in order to correct for a paramagnetic impurity. Since the ϑ values of these impurites varied between −5 and −40 K, it is conceivable that odd-numbered polyiron-containing species are present, which are antiferromagnetically coupled. The results are summarized in Table IX; Figures 6 and 7 show two representative plots of χ_M vs T for complexes of the type $L_2Fe_2(\mu\text{-}O)(\mu\text{-}XO_4)_2$, i.e., **3**, and $L_2Fe_2(\mu\text{-}XO_4)_3$, i.e., **8**. The J values found for the μ-oxo–diiron(III) complexes range from −70 cm^{-1} for **4** to −124 cm^{-1} for **5**, which indicate strong intramolecular antiferromagnetic coupling via a superexchange mechanism of two high-spin ferric ions.[42] They agree well with the value of −98 cm^{-1} reported for Lippard's (μ-oxo)bis(μ-diphenylphosphato)diiron(III) complex.[22]

In particular, for all complexes reported to date containing the (μ-oxo)bis(μ-phosphato)diiron core, the observed J values are in the rather narrow range of −80 to −98 cm^{-1}. These values differ considerably from the estimated value of −150 cm^{-1} measured for the oxidized phosphate complex from bovine spleen.[7,9,19] The origin of this strong coupling is not clear at all since coupling constants between −120 and −135 cm^{-1} have been observed in only very few binuclear model compounds which contain (i) a single oxo bridge and unsymmetrically coordinated ferric ions[43] or (ii) multiply bridged ferric ions.[26b,44] On the other hand, Lippard's complex[22] and complexes **2** and **3** do model the Fe···Fe and Fe···P distances in the oxidized phosphate complex from bovine spleen and porcine uterus[17,18] very well. The extent of exchange coupling in oxo-bridged diiron(III) complexes depends strongly on the Fe–O_{oxo} bond distance and to a lesser degree on the Fe–O–Fe angle.[45,46] Short Fe–O_{oxo} bonds enhance the coupling. Both Lippard's complex[22] and **2** have Fe–O_{oxo} bond lengths at the longer extremity as compared to other binuclear diiron(III) complexes, and, consequently, the coupling is smaller. This would indicate that the Fe–O_{oxo} bond in the oxidized phosphate complex of the beef spleen phosphatase is quite short. Removal of the oxo bridge and substitution by a third HPO_4^{2-}, $HAsO_4^{2-}$, or CrO_4^{2-} bridge as in complexes **6**, **7**, and **8** leads to dramatically reduced spin-exchange coupling. Thus, the observed J values range from −1.0 to −7.5 cm^{-1}. Tetrahedral oxoanions are poor mediators for the superexchange mechanism. These results clearly show that upon addition of phosphate or arsenate to the biomolecules the Fe–O–Fe unit is retained.

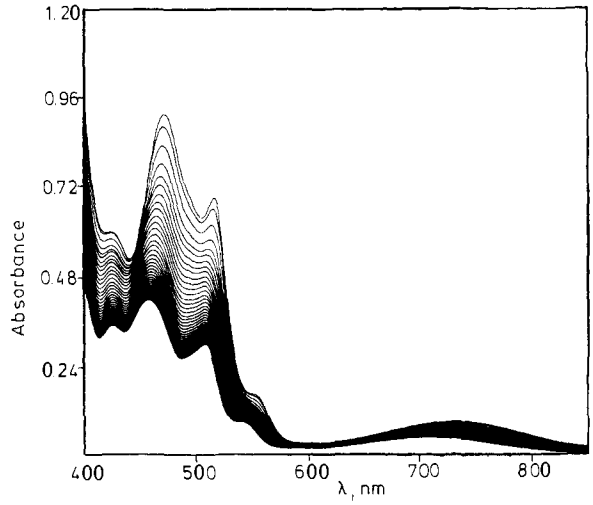

Figure 8. Repetitive scan spectrum of the hydrolysis of **1** at pH = 8 (borate/NaOH buffer; I = 0.25 M) at 25 °C; [**1**] = 6 × 10^{-4} M; [ac$^-$] = 10^{-2} M. Spectra were recorded at 1-min intervals.

Solution Behavior of $[L_2Fe_2O(O_2CCH_3)_2]^{2+}$ (1). The electronic spectrum of $[L_2Fe_2O(O_2CCH_3)_2](ClO_4)_2\cdot H_2O$ (**1**) dissolved in water (pH ≈ 7) did not change at 25 °C over a period of 24 h; it is identical with the spectrum of **1** dissolved in acetonitrile. It is concluded that **1** is stable at 25 °C and pH = 7.0 and no significant dissociation of the (μ-oxo)bis(μ-carboxylato)diiron core occurs. This is in contrast to the behavior of the corresponding complex (μ-oxo)bis[(μ-acetato)(1,4,7-triazacyclononane)iron(III)]$^{2+}$, which has been shown to undergo considerable hydrolysis in aqueous solution.[21] The methylated capping ligand in **1** is sterically more demanding than its unmethylated analogue, thereby providing an increased stability of this species in water.[34]

Addition of OH$^-$ to such an aqueous solution of **1** causes a dramatic change of the spectrum of **1** within minutes. A typical repetitive scan spectrum at pH = 8.0 is shown in Figure 8. Addition of sodium acetate (large excess) to such an alkaline solution reconstitutes the original spectrum of **1** quantitatively. This behavior indicates that there is an equilibrium between **1**, OH$^-$, uncoordinated acetate, and a hydrolyzed form of **1**. Reconstitution of **1** by addition of acetate ions in the pH range 7.5–10 occurs also on the time scale of minutes. Thus, it is conveniently possible to measure the equilibrium kinetics and to determine stability constants spectrophotometrically.

Kinetic Measurements. Kinetic measurements of the equilibrium reaction of **1** in alkaline aqueous solution were performed spectrophotometrically by following the decrease of absorbance as a function of time at λ = 460 nm. The [OH$^-$] concentration was varied from 3.0 to 160 × 10^{-7} M using noncoordinating buffer solutions (borate/$HClO_4$/NaOH and substituted lutidine[33] buffers, I = 0.25 M), and the concentration of [**1**] = 10^{-3} M was kept constant in all individual experiments. The acetate concentration was adjusted to 10^{-2} M (10-fold excess over [**1**]). A plot of k_{obsd} (s^{-1}) vs [OH$^-$] is not linear (Figure 9a) and exhibits an intercept, k_c (s^{-1}), at pH = 7; the plot of $(k_{obsd} - k_c)^{-1}$ vs [OH$^-$]$^{-1}$ is linear. From a linear regression analysis the intercept, a, and slope, b, in Figure 9b were determined to be a = 147 (5) s, b = 4.65 (6) × 10^{-6} M s, which yield values of 6.8 × 10^{-3} s^{-1} for k_2 and 2.15 × 10^5 M^{-1} s^{-1} for k_2K_1 (see below).

In a second series of experiments, [ac$^-$] was varied from 0.01 to 0.21 M by mixing at pH = 8 preequilibrated solutions of **1** with buffered (pH = 8) sodium acetate solutions. The plot of k_{obsd} (s^{-1}) vs [ac$^-$] shown in Figure 10 is linear with a small but not well-defined intercept (≈4 × 10^{-4} s^{-1}) and slope of 0.027 M^{-1} s^{-1}.

These data are in agreement with the following mechanism,

(41) McCarthy, P. J.; Güdel, H. U. *Coord. Chem. Rev.* **1988**, *88*, 69.
(42) Murray, K. S. *Coord. Chem. Rev.* **1974**, *12*, 1.
(43) Gomez-Romero, P.; DeFotis, G.; Jameson, G. B. *J. Am. Chem. Soc.* **1986**, *108*, 851.
(44) Armstrong, W. H.; Spool, A.; Papaefthymiou, G. C.; Frankel, R. B.; Lippard, S. J. *J. Am. Chem. Soc.* **1984**, *106*, 3653.
(45) Adler, J.; Ensling, J.; Gütlich, P.; Bominaar, E. L.; Gütlich, J.; Trautwein, A. X. *Hyperfine Interact.* **1988**, *42*, 869.
(46) Mukherjee, R. N.; Stack, T. D. P.; Holm, R. H. *J. Am. Chem. Soc.* **1988**, *110*, 1850.

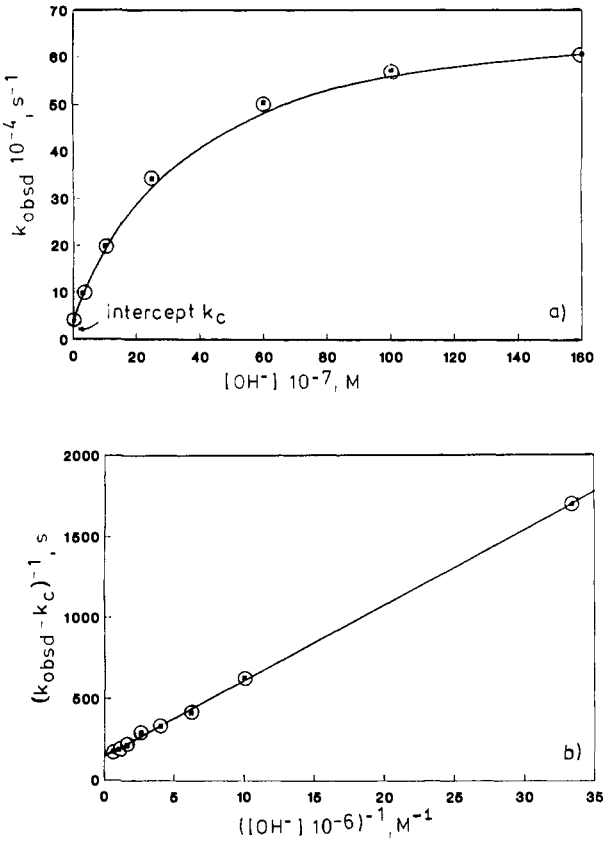

Figure 9. Kinetics of the equilibration reaction of **1** in aqueous solution at 25 °C: (a) plot of k_{obsd} vs $[OH^-]$; (b) plot of $(k_{obsd} - k_c)^{-1}$ vs $[OH^-]^{-1}$. Experimental conditions: [**1**] = 10^{-3} M = constant; [ac⁻] = 10^{-2} M = constant (I = 0.25 M; borate/NaOH buffer).

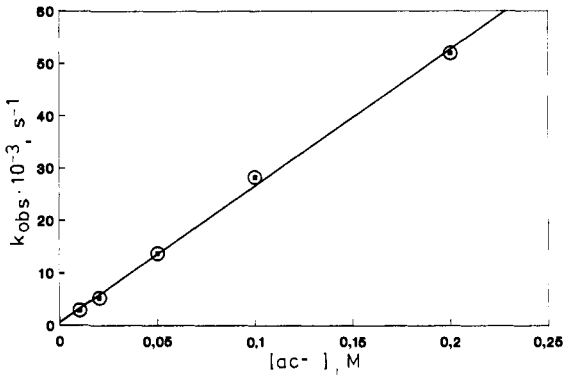

Figure 10. Kinetics of the equilibration reaction of **1** at pH = 8 (borate/NaOH buffer, I = 0.25 M) at 25 °C; plot of k_{obsd} (s^{-1}) vs [ac⁻]; [**1**] = constant = 10^{-3} M.

eq **1**, for which an equilibration rate constant, k_{eq}, as is defined in eq 2, is deduced:

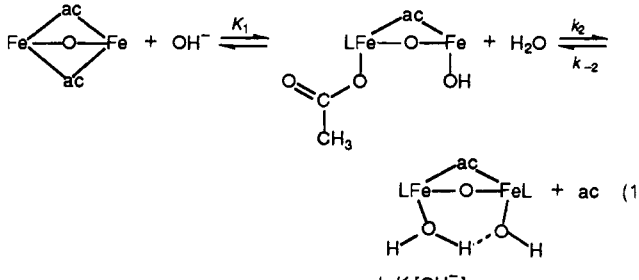

$$k_{obsd} = k_{eq} = k_{-2}[ac] + \frac{k_2K_1[OH^-]}{1 + K_2[OH^-]} \quad (2)$$

From the slope and intercept in Figure 9b, numerical values for K_1 and k_2 of 3.2 (2) × 10^5 M^{-1} and 6.8 (2) × 10^{-3} s^{-1}, respectively,

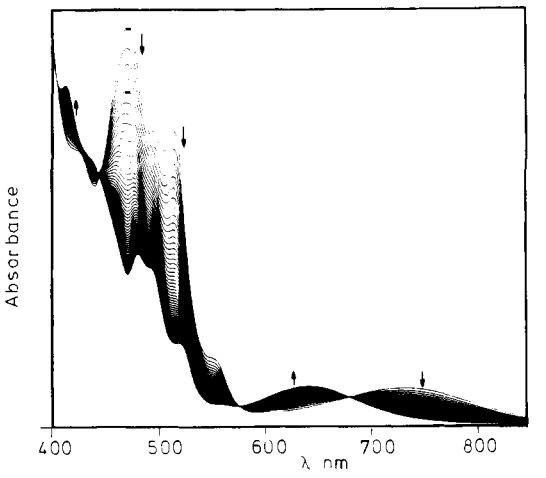

Figure 11. Repetitive scan spectrum of the reaction of **1** with $[O_3P(OC_6H_5)]^{2-}$ at pH = 8.5 and 25 °C. Spectra were recorded at 2-min intervals. Experimental conditions: [**1**] = 6 × 10^{-3} M, $[O_3POC_6H_5^{2-}]$ = 5 × 10^{-2} M, I = 0.25 M.

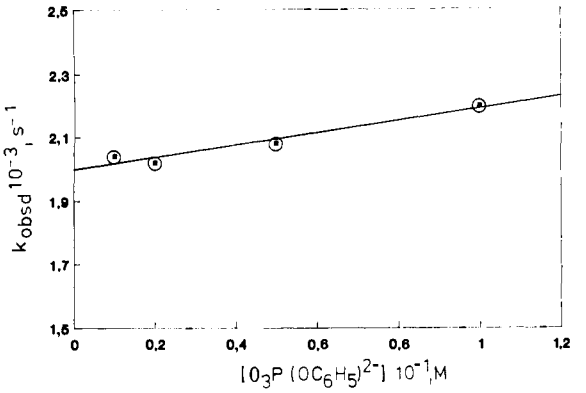

Figure 12. Plot of the observed pseudo-first-order rate constants vs $[O_3POC_6H_5^{2-}]$ for the reaction of **1** with monophenylphosphate at 25 °C. Experimental conditions: pH = 8 (borate/NaOH buffer, I = 0.25 M); [**1**] = 10^{-3} M.

at 25 °C ($I \approx 0.25$ M) were determined by a least-squares fit to the data. The slope in Figure 10 yields a numerical value for k_{-2} of 0.27 (2) M^{-1} s^{-1}. Internal consistency was established by the fact that the observed intercept, k_c, in Figure 9a of 3.9 × 10^{-4} s^{-1} at [ac] = 0.01 M agrees with the calculated value k_{-2}[ac] of 2.7 × 10^{-4} s^{-1}. The discrepancy of these two values is due to the experimental uncertainty in defining the intercept in Figure 9a. Finally the intercept in Figure 10 is smaller than 3 × 10^{-3} s^{-1}, which is in agreement with the calculated value of 2.2 × 10^{-3} s^{-1} when using eq 2.

The kinetics of the reaction between **1** and $O_3P(OC_6H_5)^{2-}$ (pH = 8, 25 °C, I = 0.25 M), generating **2**, have been measured by following the decrease of absorbance at 460 nm as a function of time. A repetitive scan spectrum (Figure 11) exhibits three isosbestic points at 410, 451, and 575 nm; the final spectrum is identical with that of **2**. The acid dissociation constants of $H_2[O_3P(OC_6H_5)]$ are pK_a^1 = 0.80 and pK_a^2 = 5.63.[47] Thus, at pH = 8, the only species present in solution is the dianion $O_3P(OC_6H_5)^{2-}$, the concentration of which was varied from 0.01 to 0.12 M and [**1**] = 10^{-3} M = constant (pseudo-first-order conditions). Aqueous solutions of **1** were mixed with buffered borate/NaOH) solutions containing $Na_2[PO_3(OC_6H_5)]$. Figure 12 shows a plot of the observed first-order rate constant, k_{obs}, vs $[O_3P(OC_6H_5)^{2-}]$. The reaction is nearly zeroth-order in $[O_3P(OC_6H_5)^{2-}]$; the intercept of 2.0 × 10^{-3} s^{-1} agrees well with the calculated value of 2.2 × 10^{-3} s^{-1} obtained from eq 2 with pH = 8 and [ac] = 0. The rate-determining step, k_2, of the reaction

(47) King, E. J.; Delory, G. E. *Biochem. J.* **1939**, *33*, 1185, 1188.

Scheme I

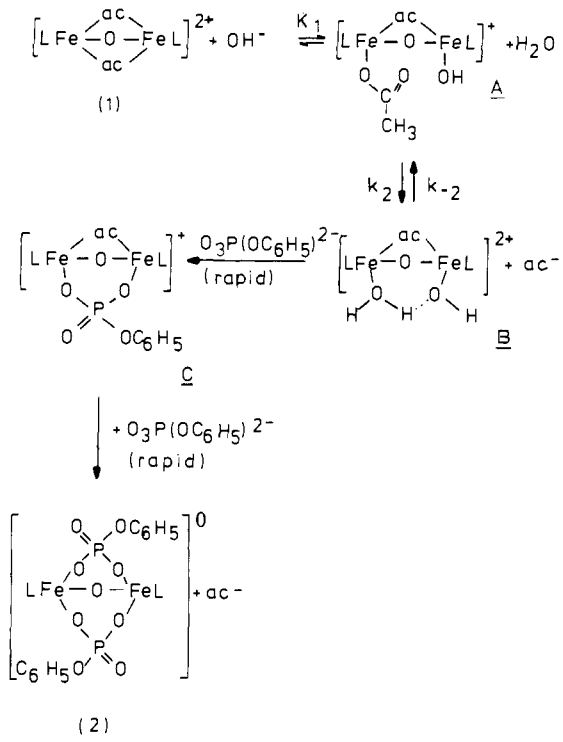

shown in Scheme I is the formation of species B. The very small dependence of the rate of formation of **2** on $[O_3P(OC_6H_5)^{2-}]$ may be due to the subsequent reaction of species C with $O_3P(OC_6H_5)^{2-}$. The rate of the second substitution reaction (C → **2**) may be of similar magnitude as the rate of formation of B.

Interestingly, complexes **3**, **4**, and **5** also form the reaction of **1** with the respective oxoanions HPO_4^{2-}, $HAsO_4^{2-}$, and CrO_4^{2-} at pH 8. The reaction mechanism proposed in Scheme I may therefore also be operative in these instances.

Spectrophotometric Determination of Stability Constants. The hydrolysis reaction of **1** in aqueous solution formulated in eq 1 involves the formation of an intermediate species A (Scheme I) containing a monodentate acetato ligand and a coordinated hydroxide. Species A hydrolyzes then with dissociation of the acetato ligand and formation of species B. This proposed Scheme I involves the equilibria shown in eq 3 and 4.

$$\mathbf{1} + OH^- \rightleftharpoons A \qquad K_1 = \frac{[A]}{[\mathbf{1}][OH^-]} \tag{3}$$

$$A \rightleftharpoons B + ac \qquad K_2 = k_2/k_{-2} = \frac{[B][ac^-]}{[A]} \tag{4}$$

The absorbance, E, in the visible is then given by eq 5, where ϵ_1, ϵ_A, and ϵ_B represent the molar absorption coefficients of species **1**, A, and B (Scheme I), respectively.

$$E = \epsilon_1[\mathbf{1}] + \epsilon_A[A] + \epsilon_B[B] \tag{5}$$

Equations 3–5 may be combined as in eq 6 and 7 by considering that the total iron concentration is given by $[Fe]_t = [A] + [B] + [\mathbf{1}]$.

$$E = [\mathbf{1}]\{\epsilon_1 + \epsilon_A K_1[OH^-] + \epsilon_B K_1 K_2[OH^-][ac^-]^{-1}\} \tag{6}$$

$$[Fe]_t = [\mathbf{1}]\{1 + K_1[OH^-] + K_1K_2[OH^-][ac^-]^{-1}\} \tag{7}$$

Combination of eq 6 and 7 with elimination of [**1**] yields eq 8.

$$E = [Fe]_t \frac{\epsilon_1 + \epsilon_A K_1[OH^-] + \epsilon_B K_1 K_2[OH^-][ac]^{-1}}{1 + K_1[OH^-] + K_1K_2[OH^-][ac^-]^{-1}} \tag{8}$$

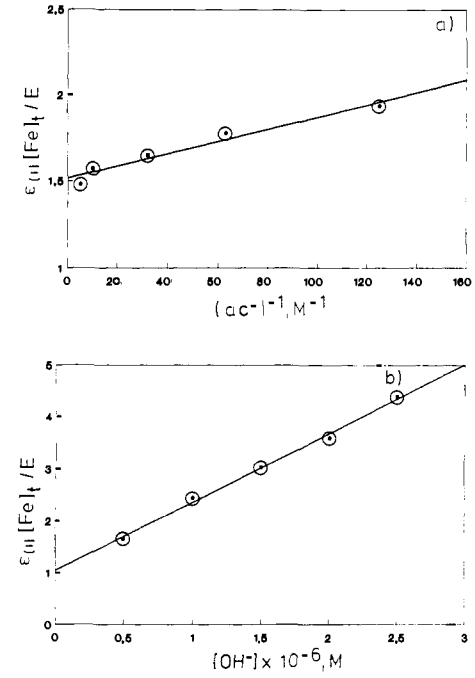

Figure 13. Spectrophotometric determination (λ = 480 nm) of stability constants of **1** in alkaline aqueous solution at 25 °C: (a) plot of $\epsilon_1[Fe]_t/E$ vs $[ac^-]^{-1}$ (E = absorbance), pH = 8; (b) plot of $\epsilon_1[Fe]_t/E$ vs $[OH^-]$; $[ac^-] = 10^{-2}$ M = constant.

If the following assumptions hold, eq 8 simplifies to eq 9: (i) $\epsilon_1 > \epsilon_A K_1[OH^-]$ and (ii) $\epsilon_1 > \epsilon_B K_2 K_1[OH^-][ac^-]^{-1}$.

$$E = [Fe]_t \frac{\epsilon_1}{1 + K_1[OH^-] + K_1K_2[OH^-][ac^-]^{-1}} \tag{9}$$

Under our experimental conditions, both assumptions most probably hold because the products $K_1[OH^-]$ and $K_2K_1[OH^-][ac^-]^{-1}$ are smaller than unity. Dissociation of both carboxylate bridges of the (μ-oxo)bis(μ-carboxylato)diiron(III) core would lead to a loss in intensity of the absorption maxima which are due to CT (or SEP) $Fe–O_{oxo}$ bands in the visible and $\epsilon_1 > \epsilon_A, \epsilon_B$. For example, the absorption spectrum of $[L_2Fe_2(acac)_2(\mu\text{-}O)]^{2+}$ is featureless in the 450–900-nm region[48] (acac = acetylacetonate(1−)). On the other hand, Que's complex $[Fe_2(TPA)_2O(OBz)]^{3+}$ with a (μ-oxo)(μ-benzoato)diiron(III) core shows spectral features similar to those of the (μ-oxo)bis(μ-carboxylato)diiron complexes.[49] Therefore, we point out that the structures for A in B given in Scheme I are by no means established. Loss of both acetato ligands from **1** is not supported by the equilibration kinetics (first-order dependence on $[ac^-]$) nor the present equilibrium study.

Equation 9 is then rewriten as in eq 10a or 10b. The absorbances of equilibrated solutions of **1** at (i) constant pH = 8 and

$$\frac{\epsilon_1[Fe]_t}{E} = 1 + K_1[OH^-] + K_1K_2[OH^-][ac^-]^{-1} \tag{10a}$$

$$\frac{\epsilon_1[Fe]_t}{E} = (K_1 + K_1K_2[ac^-]^{-1})[OH^-] + 1 \tag{10b}$$

$[ac^-]$ in the range 0.008–0.2 M and (ii) at $[ac^-]$ = constant = 0.01 M and $[OH^-]$ in the range 0.5×10^{-6}–2.5×10^{-6} M (borate buffer) were measured. Plots of $\epsilon_1[Fe]_t/E$ vs $[ac^-]^{-1}$ and $\epsilon_1[Fe]_t/E$ vs $[OH^-]$ should be linear. This has been observed as is shown in Figure 13. From the slopes and intercept, numerical values

(48) Wieghardt, K.; Pohl, K.; Bossek, U.; Nuber, B.; Weiss, J. *Z. Naturforsch.* **1988**, *43b*, 1184.

(49) (a) Yan, S.; Que, L., Jr.; Taylor, L. F.; Anderson, O. P. *J. Am. Chem. Soc.* **1988**, *110*, 5222. (b) Yan, S.; Cox, D. D.; Pearce, L. L.; Juarez-Garcia, C.; Que, L., Jr.; Zhang, I. H.; O'Connor, C. *Inorg. Chem.* **1989**, *28*, 2507.

for K_1 and K_2 were evaluated from a least-squares fit to the data to be 5.5 (7) × 10^5 M^{-1} and 1.4 (5) × 10^{-2} M, respectively. Both values are in reasonable agreement with those obtained from the kinetic measurements of the equilibration reaction of **1** (K_1 = 3.2 × 10^5 M^{-1} and k_2/k_{-2} = K_2 = 0.025 M).

Summary and Conclusions

Two related series of complexes containing the (μ-oxo)bis(μ-XO_4)Fe^{III}_2 core with XO_4 = $O_3P(OC_6H_5)^{2-}$, HPO_4^{2-}, $HAsO_4^{2-}$, and CrO_4^{2-} (type A) or, alternatively, the tris(μ-XO_4)Fe_2 unit with XO_4 = $O_3P(OC_6H_5)^{2-}$, HPO_4^{2-}, and $HAsO_4^{2-}$ (type B) have been synthesized. Their electronic spectra and magnetic properties have been studied. The following conclusions are derived:

(1) Complexes of type A display rich electronic spectra in the near-UV, visible and near-IR. In contrast, type B complexes are featureless in the visible and near-IR, exhibiting only one charge-transfer absorption in the near-UV.

(2) In complexes of type A, strong intramolecular antiferromagnetic coupling of the high-spin ferric ions is observed via a superexchange mechanism mediated by the single atom bridge (J, −80 to −120 cm^{-1}). In type B complexes, very weak antiferromagnetic coupling is observed (J, −7.5 to −2.0 cm^{-1}).

(3) The (μ-oxo)bis(μ-phosphato)diiron complexes **2** and **3** model the known structural and to some degree the physical properties of the oxidized uteroferrin phosphate complex. The Fe···Fe and Fe···P distances in both the model compounds and the biomolecules are very similar, which suggests the presence of an Fe–O–Fe unit and bidentate bridging phosphate in the biomolecule.

(4) The very strong exchange coupling observed for the purple, oxidized phosphate containing enzyme from bovine spleen with a lower limit of $-2J \geq 300$ cm^{-1} is proposed to be indicative of very short $Fe–O_{oxo}$ bonds (≈1.78 Å).[50] In the μ-phosphato model complexes, this bond is longer (1.82 Å), and consequently, the exchange coupling is weaker.

Finally, the first kinetic and equilibrium study of a complex containing the (μ-oxo)bis(μ-carboxylato)diiron core has been carried out. This unit has been identified in the oxidized form of hemerythrin, and possibly ribonucleotide reductase[3] (**1**) hydrolyses in alkaline aqueous solutions with dissociation of one acetato group. The resulting (μ-oxo)(μ-acetato)diiron(III) species is reactive toward nucleophiles such as $O_3P(OC_6H_5)^{2-}$, HPO_4^{2-}, and $HAsO_4^{2-}$. The formation of **2** from **1** was found to be independent of the $O_3P(OC_6H_5)^{2-}$ concentration; the formation of the (μ-oxo)(μ-acetato)diiron species is rate determining.

These observations raise the possibility that binding of phosphate to the enzyme uteroferrin occurs with concomitant displacement of μ-carboxylato bridges.

Acknowledgment. This work was supported by the Fonds der Chemischen Industrie. We thank Professor Joann Sanders-Loehr (Oregon Research Center) for communication of results prior to publication.

Supplementary Material Available: Tables S1–S12 and Tables II–VII listing bond distances, bond angles, anisotropic displacement parameters, and calculated positional parameters for hydrogen atoms of complexes **2**, **5**, and **8**, Table S13 listing proposed hydrogen positions of hydrogen bonds in **8**, and Table S14 listing kinetic data (18 pages). Ordering information is given on any current masthead page.

(50) The general problem of the distance dependence of the exchange coupling constant J for Fe^{III}–O–Fe^{III} complexes has been discussed: Gorun, S. M.; Lippard, S. J. *Recl. Trav. Chim. Pays-Bas* **1987**, *106*, 416.

Nonequilibrium Transition-State Solvation and Marcus Work Terms. Comparison of Their Contributions to Solvent Effects on Intrinsic Rate Constants for Proton Transfers

Joseph L. Kurz

Contribution from the Department of Chemistry, Washington University, St. Louis, Missouri 63130. *Received January 26, 1989*

Abstract: Within the context of his principle of nonperfect synchronization, Bernasconi explained H_2O/Me_2SO solvent effects on intrinsic rate constants (k_0s) for proton transfer ($AH + B^- \rightarrow A^- + HB$) as the result of nonequilibrium transition-state (TS) solvation that arises from asynchrony between transfer of charge and reorganization of the solvation of that charge during the transfer step ($AH,B^- \rightarrow A^-,HB$); such nonequilibrium solvation would contribute a solvent-dependent addition to the intrinsic barrier ($\Delta G_0^{\ddagger}$). When AH is uncharged and B^- is an anion (or an uncharged solute with a tightly solvated basic electron pair), an alternative origin exists: as defined by Bernasconi, k_0 is a function of the Marcus work term (w^r) as well as of $\Delta G_0^{\ddagger}$, so that an observed solvent effect on k_0 could result from the partial desolvation of B^- that must accompany formation of the precursor complex ($AH + B^- \rightleftharpoons AH,B^-$); this desolvation would contribute a solvent-dependent addition to w^r. Analogous ambiguities concerning the origins of observable differences between k_0s also exist for other charge-transfer reactions, including electron transfers. The separate contributions to solvent effects on k_0 that arise from the solvent dependencies of w^r and $\Delta G_0^{\ddagger}$ are here estimated by modeling the charged solutes (B^-, precursor complex, and TS) as charges inside spherical or ellipsoidal cavities in dielectric continua. Free energies of TS models containing nonequilibrium polarization of those continua are calculated by Marcus' method. Calculations based on these models predict values of the H_2O/Me_2SO solvent effect on k_0s for proton transfers from uncharged AHs to RCO_2^- that are consistent with observed values and are composed of approximately equal contributions from those two sources. They also predict that, if significant charge/solvation disequilibrium really is present in the TS, then k_0 for a proton transfer of this charge type in Me_2SO should be larger than k_0 for the same transfer in MeCN; observation of this direction of this solvent effect could not be explained if all solutes were assumed to have equilibrated solvation, but would be consistent with the proposed nonequilibrium TS solvation.

Asynchrony between transfer of charge in a chemical reaction and reorganization of the solvation of that charge can result in nonequilibrium solvation in the transition state (TS). Since the free energy required for complete desolvation of an ion in a polar solvent is very large (ca. 50–100 kcal mol^{-1} for singly charged ions), the disequilibrium that could result from even a relatively small charge transfer/solvation asynchrony might be expected to make a significant addition to the barrier height ($\Delta G^{\ddagger}$) for the reaction.

0002-7863/89/1511-8631$01.50/0